Analyst

Detection of 15N-labeled Metabolites in Microbial Extracts using AI-Designed Broadband pulses for 1H, 15N Heteronuclear NMR Spectroscopy

Journal:	*Analyst*
Manuscript ID	AN-ART-01-2025-000074.R3
Article Type:	Paper
Date Submitted by the Author:	17-Mar-2025
Complete List of Authors:	Manu, V.; University of Minnesota Medical School Twin Cities, Biochemistry, Molecular Biology and Biophysics Tonelli, Marco; University of Wisconsin-Madison, Biochemistry Bailey, Ann Bell; University of Wisconsin-Madison, Chemistry Sharma, Alok ; National Cancer Institute Frederick National Laboratory for Cancer Research Bugni, Tim; University of Wisconsin Madison, School of Pharmacy Veglia, Gianluigi; University of Minnesota Twin Cities, Biochemistry, Molecular Biology & Biophysics

Detection of ^{15}N-labeled Metabolites in Microbial Extracts using AI-Designed Broadband Pulses for ^{1}H, ^{15}N Heteronuclear NMR Spectroscopy

Manu V.S.,[1] Marco Tonelli,[2] Bailey Bell,[3] Alok K. Sharma,[4] Tim S. Bugni,[3,4,5] and Gianluigi Veglia[1]*

[1] Department of Biochemistry, Molecular Biology & Biophysics, University of Minnesota, Minneapolis, Minnesota 55455, United States
[2] Department of Biochemistry, University of Wisconsin-Madison, 433 Babcock Drive, Madison, Wisconsin, 53706, USA.
[3] Pharmaceutical Sciences Division, University of Wisconsin–Madison, Madison, WI, USA
[4] NCI RAS Initiative, Cancer Research Technology Program, Frederick National Laboratory for Cancer Research, Leidos Biomedical Research, Inc., Frederick, MD 21701, USA
[5] Small Molecule Screening Facility, UW Carbone Cancer Center, Madison, WI, USA
[6] Lachman Institute for Pharmaceutical Development, University of Wisconsin–Madison, Madison, WI, USA

ABSTRACT: Approximately 40% of bacterial and mammalian metabolites contain nitrogen-based chemical moieties such as amides, amines, and imines. The identification and quantification of these groups via 2D ^{1}H,^{15}N heteronuclear NMR spectroscopy have broadened the catalog of NMR-detected metabolites. However, these NMR experiments necessitate broadband radiofrequency (RF) pulses for inversion and refocusing operations to encompass the full range of ^{15}N chemical shifts, a challenge that becomes increasingly apparent at high and ultra-high magnetic fields. Here, we show that a newly AI-designed broadband ^{15}N universal 180° pulse for both inversion and refocusing incorporated in the 2D ^{1}H, ^{15}N heteronuclear single quantum coherence (2D ^{1}H-^{15}N BB-HSQC) experiment significantly enhances spectral sensitivity. We demonstrate the advantage of the new technique by analyzing the crude extract of *Micromonospora* sp. WMMC264, a microbial strain that produces siderophores for iron absorption from the environment. The implementation of the AI-designed pulse in the 2D ^{1}H-^{15}N BB-HSQC experiment will contribute to advancing the analysis of nitrogen-containing metabolites in biological fluids and cell extracts.

INTRODUCTION

Isotopic labeling has significantly enhanced the repertoire of metabolites available for tracing microbial and mammalian metabolism.[1-2] Notably, cultures of bacteria labeled with ^{15}N have facilitated the identification of nitrogen-bearing chemical moieties, including functional groups such as amides, amines, and imines.[3-5] These chemical moieties are found in a range of compounds, from low-molecular-weight molecules such as hormones, amino acids, neurotransmitters, antioxidants, and osmolytes, to larger biomacromolecules and their complexes.[5] It has been estimated that more than 40% of metabolites contain nitrogen-bearing chemical moieties.[5] However, many of the NMR experiments designed for ^{15}N detection are primarily geared towards structural biology and are inadequate for thorough metabolite analysis. In particular, the detection of ^{15}N labeled metabolites requires broadband RF pulses to perform operations such as magnetization inversion and refocusing over a large ^{15}N chemical shift breadth. To overcome this hurdle, we utilized the GENETICS-AI (or GENErator of TrIply Compensated RF pulSes via Artificial Intelligence) software[6-7] and designed a universal 180° pulse able to cover the entire ^{15}N bandwidth for both inversion and refocusing operations. The GENETICS-AI pulses are highly compensated for field inhomogeneity and possess high-fidelity operation across the irradiated bandwidth.[6] We modified the basic heteronuclear single quantum coherence (HSQC) experiments implementing our universal 180° pulse and analyzed the crude extract of *Micromonospora* sp. WMMC264, a microbial strain that produces siderophores for iron absorption from the environment.[8] Specifically, we compared three 2D ^{1}H,^{15}N HSQC experiments implemented with commonly used refocused and inversion pulses with our variant implemented with the GENETICS-AI designed pulses. We found that the signals of the metabolites from the crude microbial extracts acquired with our new universal 180° pulse are significantly more intense than those obtained with the commonly used broadband pulses. The implementation of the GENETICS-AI pulses into the 2D ^{1}H-^{15}N HSQC sequence will advance the analysis of nitrogen-containing metabolites in biological fluids and cell extracts .

EXPERIMENTAL SECTION

Bacterial Fermentation. To make artificial seawater, solution I (415.2 g NaCl, 69.54 g Na_2SO_4, 11.74 g KCl, 3.40 g $NaHCO_3$, 1.7 g KBr, 0.45 g H_3BO_3, 0.054 g NaF per liter) and solution II (187.9 g $MgCl_2{\bullet}6H_2O$, 22.72 g $CaCl_2{\bullet}2H_2O$, 0.428 g $SrCl_2{\bullet}6H_2O$ per liter) were prepared separately and combined to achieve a total volume of 20 L. To generate extracts, a 10 mL seed culture in DSC medium (20 g soluble starch, 10 g glucose, 5 g peptone, 5 g yeast extract per liter of 50% artificial seawater) was inoculated with *Micromonospora* sp. WMMC264 and shaken (200 rpm at 28 °C) for 5 days. ^{15}N-labeled cultures were then prepared by inoculating two 100 mL flasks containing 25 mL ^{15}N-labeled ASW-A medium (20 g soluble starch, 10 g glucose, 5 g $CaCO_3$, 5 g yeast extract, 2.5 g peptone, 2.5 g ^{15}N-labeled ammonium chloride per liter of artificial seawater) with Diaion HP20 (7% by weight), one of which also contained 50 μM iron (III) sulfate, with 2 mL seed culture. Cultures were allowed to grow for 2 weeks at 28 °C. After this step, resin and cells were removed and extracted 3x with 20 mL acetone. Cloning, overexpression, and purification of the recombinant NRAS(1-169)^{Q61R} were conducted as previously reported.[9-11] In brief, the DNA sequence encoding the His6-MBP-TEV-Hs.NRASQ61R construct (where MBP refers to maltose-binding protein and TEV is the tobacco etch virus protease recognition sequence) was ligated into a plasmid and transformed into competent V. *natriegens* cells. The uniformly labeled ^{13}C/^{15}N NRAS(1-169)^{Q61R} was overexpressed by culturing bacterial cells in ModM9 medium, which contained ^{13}C-glucose and $^{15}NH_4Cl$ as the sole sources of ^{13}C and ^{15}N, respectively. The protein was purified using Immobilized Metal Affinity Chromatography (IMAC) followed by Size Exclusion Chromatography (SEC). The purified NRAS(1-169)^{Q61R} was stored in a buffer solution containing 20 mM HEPES (pH 7.4), 150 mM NaCl, 1 mM $MgCl_2$, and 1 mM TCEP. The purified NRAS(1-169)^{Q61R} was then saturated with guanosine triphosphate (GTP). The saturation of the protein by

GTP was assessed via HPLC and mass spectrometry. The NMR samples were quickly concentrated and flash-frozen before further use.

Sample Preparation and NMR Spectroscopy. Cell extracts were processed by solid phase extraction to remove salts. Briefly, extracts were dissolved in 2 mL 10% aqueous CH_3OH and loaded onto a 500 mg C18 column. The column was washed with 2 mL H_2O followed by 2 mL 90% aqueous CH_3OH. The organic fraction was then dried and resuspended in 170 µL DMSO-d6 for NMR analysis. A 0.8 mM sample of $NRAS^{Q61R}$-GTP (MW 20.3 kDa) was prepared in a buffer containing 93% H_2O/7% D_2O in 20 mM MES-d_{13} (pH 6.5), 50 mM NaCl, 100 mM KCl, 2 mM $MgCl_2$, 1 mM TCEP-d_{16}, and 500 µM 2,2-dimethyl-2-silapentanesulfonic acid (DSS) as an internal standard. Two-dimensional (2D) ^{1}H-^{15}N HSQC spectra for the ^{15}N metabolites were acquired at 288.2 K on a 600 MHz spectrometer equipped with a CP TCI 600S3 H&F-C/N-D-05 Z probe (Z129649_0030). Sixteen transients were averaged over 128 dummy scans with a 1.0 s relaxation delay. The NMR data were collected using 768 (direct) × 310 (indirect) complex points, corresponding to acquisition times of 76.8 ms (^{1}H, 16.66 ppm spectral width) and 40.3 ms (^{15}N, 126.49 ppm spectral width). The receiver gain was set to 128.0. The total acquisition time was 3 h 8 m. All NMR data were processed using NMRPipe.[12] In the direct (^{1}H) dimension, an exponential apodization window function with 10 Hz line broadening was applied, followed by zero-filling to 2048 points and Fourier transformation. In the indirect (^{15}N) dimension, a shifted sine window function (off = 0.5, end = 0.99, power = 2) was applied prior to zero-filling to 1024 points and Fourier transformation. Subsequently, polynomial baseline correction was performed in the indirect dimension using an automatic algorithm to determine the optimal zero-order polynomial for removal of residual baseline offsets.

Design of RF pulse for broadband inversion and refocusing operations. The broadband pulse UR33, designed for spin refocusing and inversion operations, was created using GENETICS-AI.[6] This software optimizes the RF phase shape for the 180-degree pulse operator, represented as $\exp(-i\pi I_x)$, where I_x is the Pauli spin operator. GENETICS-AI employs a large library of RF shapes (~1,000,000) generated through the evolutionary algorithm. A neural network, trained on this RF pulse library, generates additional pulse shapes, which are further refined to achieve the optimal solution. The UR33 shape (universal 180° pulse) produced for the ^{15}N inversion and refocusing operations spans a bandwidth of approximately 400 ppm (on a 600 MHz spectrometer). The UR33 is part of a broader family of pulses we previously designed for universal 180° flipping operation.[6]

RESULTS

To evaluate the effects of broadband pulses on the ^{15}N bandwidth, we started from the original sensitivity-enhanced ^{1}H-^{15}N HSQC (heteronuclear single quantum coherence, Bruker library entry: hsqcetf3gpsi2) pulse scheme.[13-14] To eliminate artifacts and improve coherent selection, we modified the original sequence by flanking the refocusing pulses with gradients in the first INEPT block. We also included two weak bipolar gradient pulses during the t_1 incrementation period. **Figure 1A** displays the ^{1}H,^{15}N HSQC experiment in which the unfilled rectangles represent the 90° hard pulses on both ^{1}H and ^{15}N channels. Note that the lighter green pulses perform an inversion operation on the longitudinal component of the ^{15}N magnetization ($M_z \rightarrow -M_z$), whereas the darker green pulses are used for refocusing the transverse components ($M_y \rightarrow -M_y$ and $M_x \rightarrow M_x$ if the RF pulse is applied along the x axis). To assess the performance of the UR33 pulse, we tested different pulse shapes, including an adiabatic secant pulse (HypSec.500),[15-16] a CHIRP pulse (Crp20,1,40.1),[17] a composite CHIRP pulse (Crp60comp.4),[17] The amplitude and phases of all these pulses are reported in **Figures 1B-1E**, whereas their simulated and experimental offset responses are shown in **Figures 2** and **S1**. The 2D response profiles of these shapes vs. RF amplitude and offsets are shown in **Figure S2,** showing an effective performance even with B_1 field inhomogeneity compensation of ±10%. First, we modified the ^{1}H,^{15}N HSQC experiment including a hard pulse for refocusing the transverse magnetization, and an adiabatic secant pulse, HypSec.500, for inverting the longitudinal magnetization (bbhsqcetf3gpsi2.1). Note that the use of hard pulse is necessary as the HypSec.500 pulse is not efficient for refocusing operations. Then, we implemented the 2D ^{1}H,^{15}N HSQC experiment with CHIRP pulses (Crp20,1,40.1) for inversion and a composite CHIRP pulse(Crp60comp.4) for refocusing (bbhsqcetf3gpsi2.2). Finally, we used the new AI-designed UR33 pulse for both inversion and refocusing operations (bbhsqcetf3gpsi2.3). The simulated responses of the magnetization components to all these pulses are illustrated in **Figure 2**. For the bbhsqcetf3gpsi2.1 sequence, both the hard pulses for refocusing and inversion operations display a bandwidth of approximately 200 ppm, which causes a loss of signal intensity at the two edges of the ^{15}N spectrum (**Figure 2A**). In contrast, the bbhsqcetf3gpsi2.2 sequence equipped with CHIRP pulses for refocusing and composite CHIRP for inversion irradiates ~300 ppm, covering the entire ^{15}N spectrum (**Figure 2B**). Similarly, the bbhsqcetf3gpsi2.3 sequence with the AI-designed UR33 pulses for both inversion and refocusing covers homogenously the entire ^{15}N bandwidth, extending to ~ 400 ppm for all the components of the magnetization (**Figure 2**).

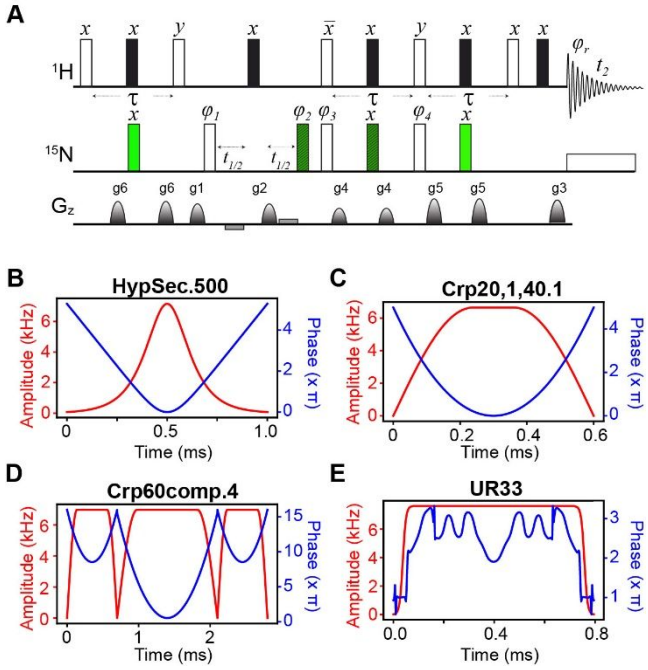

Figure 1. (A). Schematic of the modified 2D sensitivity-enhanced ^{1}H,^{15}N HSQC pulse sequences **A**. Unfilled rectangles in the ^{1}H channel denote hard 90° pulses, while filled rectangles represent hard 180° pulses. Green rectangles in the ^{15}N channel indicate inversion (filled) and refocusing (patterned) pulses. The broadband versions of ^{1}H-^{15}N SE-HSQC include: (1) bbhsqcetf3gpsi2.1, with adiabatic secant pulses (HypSec.500) for inversion and hard pulses for refocusing; (2) bbhsqcetf3gpsi2.2 using CHIRP pulses (Crp20,1,40.1) for inversion and a composite CHIRP pulse (Crp60comp.4) for refocusing; and (3) bbhsqcetf3gpsi2.3 with UR33 pulses for both inversion and refocusing operations. Phase cycling schemes are: φ1 = {x, -x}, φ2 = {x, x, x, x, y, y, y, y, y, -x, -x, -x, -y, -y, -y, -y}, φ3 = {x, x, -x, -x}, φ4 = {y, y, -y, -y}, and φ_r

= {x, -x, -x, x, -x, x, x, -x}. The inter-pulse delay τ is set to $1/2^1J_{HN}$, where $^1J_{HN}$ is the amide groups scalar coupling constant. Gradient strengths are applied in the ratio g_1: g_2: g_3: g^4: g_5: g_6 = -61: 80: 8.1: 11: 17: 23 for coherence selection and spectral sensitivity. (B) - (E) Amplitude (red) and phase (blue) shapes versus time for all inversion and refocusing pulses.

We initially tested the three 2D ^1H,^{15}N BB-HSQC pulse sequences using a 0.8 mM sample of NRAS^{Q61R}-GTP protein (20.3 kDa) and compared the intensities of the peaks observed in the corresponding ^{15}N spectra. **Figures S3-S4** shows the 1D projections as well as the 2D ^1H,^{15}N BB-HSQC spectra. Analysis of the 1D projections and the 2D peaks reveals a significant enhancement of the signals achieved through the implementation of the UR33. This signal enhancement is quantified in the histograms shown in **Figure S5 A** and **B**, where the intensity of the ^1H,^{15}N HSQC signals detected with the AI-generated pulses (I_3, bbhsqcetf3gpsi2.3) is compared to those detected using the CHIRP pulse sequence (I_2, bbhsqcetf3gpsi2.2) and the Hypersecant pulse sequence (I_1, bbhsqcetf3gpsi2.1), respectively. Overall, the bbhsqcetf3gpsi2.3 pulse sequence shows an increase of approximately 50% compared to bbhsqcetf3gpsi2.2, and an average increase of about 25% compared to bbhsqcetf3gpsi2.1. We then applied the three ^1H,^{15}N HSQC pulse sequences on the crude extract samples of *Micromonospora* sp. WMMC264 cultured with and without the presence of iron sulfate. **Figures S6-S7** display the full 2D ^1H-^{15}N BB-HSQC spectra along with their ^1H and ^{15}N projections for crude extracts of *Micromonospora* sp. WMMC264, obtained both in the absence and presence of iron using the three HSQC pulse sequences. Portions of these spectra are reported in **Figures 3**, highlighting the metabolite peaks resonating at the edge of the ^{15}N bandwidth. In particular, we examined the intensities of the resonances at the boundary of the spectral width, utilizing a hard pulse (**Figure 3A**), CHIRP pulses (**Figure 3B**), and our AI-generated pulse (**Figure 3C**). The hard inversion pulse produced the spectrum with the lowest sensitivity. Conversely, the spectrum obtained with CHIRP pulses demonstrated a notable enhancement in sensitivity. However, the greatest signal enhancement was achieved with the UR33 pulse.

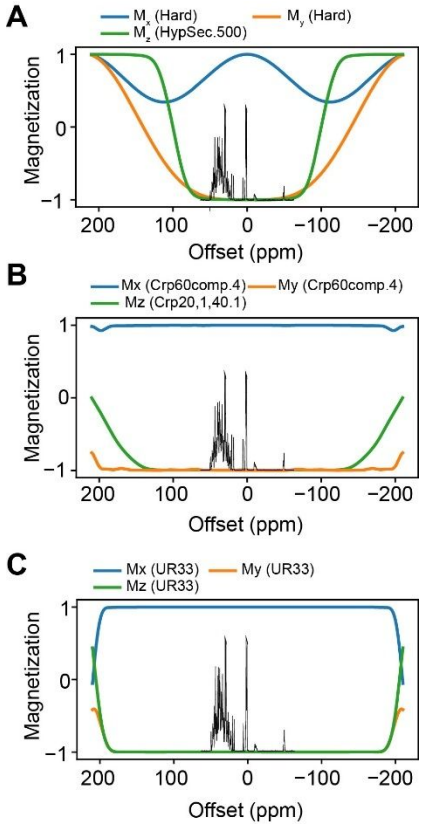

Figure 2. Offset responses of the ^{15}N inversion and refocusing pulses used for the ^1H,^{15}N SE-HSQC variants. (A) Response for the bbhsqcetf3gpsi2.1 sequence with a HypSec.500 pulse (maximum RF amplitude of 7.15 kHz and duration of 1 ms) for inversion, and a hard π pulse (RF amplitude of 7.62 kHz) for refocusing. (B) Response for the bbhsqcetf3gpsi2.2 sequence, with a Crp20,1,40.1 (maximum RF amplitude of 6.65 kHz) for inversion, and a Crp60comp.4 pulse (maximum RF amplitude of 6.98 kHz) for refocusing, with durations of 600 μs and 2.8 ms, respectively. (C) Response for the bbhsqcetf3gpsi2.3 sequence with UR33 pulses for inversion and refocusing (RF amplitude of 7.61 kHz and a pulse length of 795 μs). The ^{15}N projections from the spectra of *Micromonospora* sp. Extract acquired with bbhsqcetf3gpsi2.1, bbhsqcetf3gpsi2.2, and bbhsqcetf3gpsi2.3 are included in panels A, B and C, respectively, as a reference.

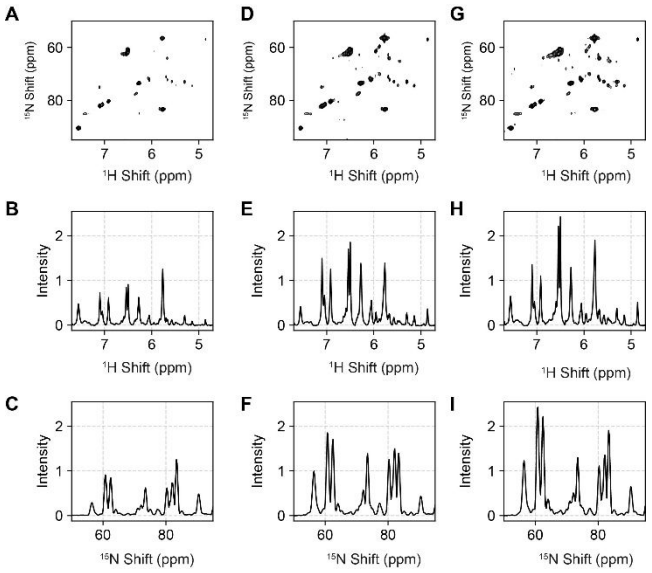

Figure 3. 2D ^{1}H,^{15}N BB-HSQC spectra of crude *Micromonospora* sp. WMMC264 extracts in the absence of iron acquired with the three pulse sequences. (A-C) Portion of the 2D spectrum and corresponding ^{1}H and ^{15}N projections acquired using a hard pulse for inversion operation; (D-F) portion of the 2D spectrum and corresponding ^{1}H and ^{15}N projections acquired with CHIRP pulses; (G-I) portion of the 2D spectrum and corresponding ^{1}H and ^{15}N projections acquired with AI-generated UR33 pulse.

Figure 4 presents a comparative analysis of the HSQC peak intensities from the crude *Micromonospora* sp. WMMC264 extracts using three different pulse sequences: bbhsqcetf3gpsi2.1, bbhsqcetf3gpsi2.2, and bbhsqcetf3gpsi2.3, where I_1, I_2, and I_3 are the respective intensities of the resulting peaks. In bacterial extracts cultured without Fe(III), the bbhsqcetf3gpsi2.3 sequence yielded a 2D spectrum with a maximum sensitivity enhancement of 286% and an average gain of 62% compared to bbhsqcetf3gpsi2.1. In contrast, the bbhsqcetf3gpsi2.3 sequence demonstrated maximum and average gains of 133% and 31%, respectively, over the bbhsqcetf3gpsi2.2 experiment. For bacterial extracts cultured with Fe(III), the bbhsqcetf3gpsi2.3 experiment showed a maximum sensitivity gain of 288% and an average gain of 77% compared to bbhsqcetf3gpsi2.1. Additionally, it exhibited maximum and average gains of 175% and 34%, respectively, compared to the bbhsqcetf3gpsi2.2 experiment. These results clearly demonstrate that the ^{1}H,^{15}N BB-HSQC spectra acquired using the AI-designed UR33 pulse for both refocusing and inversion operations provide significantly enhanced sensitivity.

DISCUSSION

The library of metabolites detectable through NMR spectroscopy is continually growing, now containing over 1,500 identifiable analytes, with many more yet identified.[18] The stable isotope resolved metabolomics (SIRM) techniques coupled to ^{13}C and ^{15}N heteronuclear NMR spectroscopy[19] have contributed to the expansion of the databases.[5]

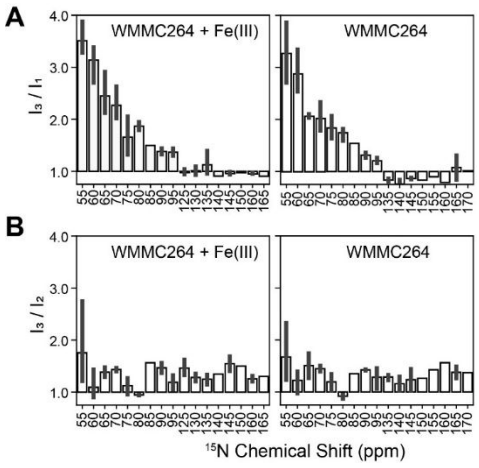

Figure 4. Sensitivity gains obtained with the bbhsqcetf3gpsi2.3 pulse sequence (peak intensity I_3) relative to (A) bbhsqcetf3gpsi2.1 (peak intensity I_1) and (B) bbhsqcetf3gpsi2.2 (peak intensity: I_2), as plotted against the ^{15}N chemical shift. Black bars indicate the range of gains when multiple resonances occur within the same chemical shift region.

Despite this progress, many hurdles remain, including NMR techniques that thus far have been optimized for biomolecular structure determination rather than metabolomics analysis. For ^{15}N NMR spectroscopy, a significant challenge is to cover the entire bandwidth. Inverse-detected 2D heteronuclear pulse sequences involve excitation, inversion, and refocusing operations that for biomolecules are performed by hard RF pulses. Whereas the 90^{o} hard pulses are able to cover the entire bandwidth, inversion and refocusing operations are more challenging to achieve using hard RF pulses. It should be noted that inversion and refocusing are two distinct operations. A refocusing operation involves flipping the nuclear spins by 180 degrees in the transverse plane, while the inversion operation flips them along the z-axis. Refocusing is often more challenging to optimize, due to its stricter requirements compared to inversion operations. Although adiabatic or CHIRP pulses can perform high-fidelity inversion, they are generally less suitable for spin refocusing.[17] Composite CHIRP pulses can also be used for refocusing operations; however, they tend to be suboptimal because of their longer duration. The ideal solution is the universal 180^{o} pulse that can flip magnetization regardless of its initial state. The UR33 pulse, generated by GENETICS-AI, meets the criteria for a universal 180^{o} pulse and can be utilized for both refocusing and inversion operations with high fidelity. As shown in **Figure 5**, the duration of the UR33 pulse is approximately one-third of the composite CHIRP pulse. This reduced duration enables it to execute high-fidelity refocusing operations more swiftly, thereby minimizing signal losses associated with spin relaxation. The benefits of this approach are evident in the signal enhancements we recorded across the entire ^{15}N spectra of our cell extracts, particularly for peaks located at the edges of the bandwidth.

Note, however, that our cell extracts were solubilized in DMSO to minimize signal losses typically associated with chemical exchanges in protic solvents. This problem is especially significant for nitrogen protons in metabolites, which are highly labile in aqueous solutions and at physiological pH.[5] A potential solution to this issue is the use of water irradiation devoid (WADE) pulses for the ^{1}H channel.[20-21] This approach would eliminate solvent irradiation, reducing the saturation effects seen with other solvent suppression methods.[20-21] Our next step will be to incorporate WADE pulses into the design of ^{1}H,^{15}N BB-HSQC experiments to be used for recording spectra on water samples.

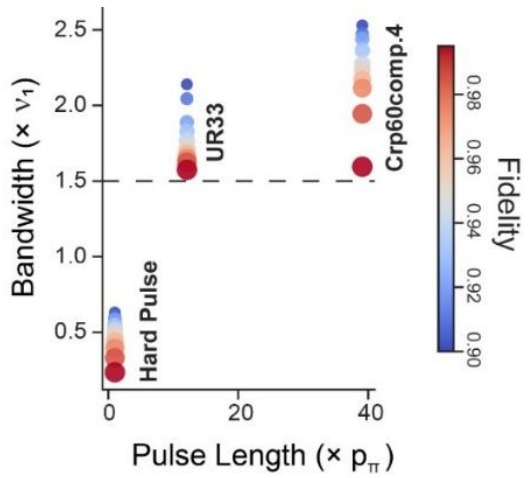

Figure 5. Comparison of the performance of the different RF pulses utilized for 2D $^{1}H,^{15}N$ BB-HSQC sequences. The hard pulse has the shortest duration but can cover only a limited ^{15}N bandwidth. On the opposite end, composite CHIRP pulses cover a larger bandwidth but with significantly longer pulse duration. UR33 covers the same bandwidth of composite CHIRP pulse with approximately 1/3 of the pulse length.

CONCLUSIONS

In summary, we demonstrate that a newly developed AI-designed inversion and refocusing pulse, integrated into a classical 2D $^{1}H,^{15}N$ HSQC NMR pulse sequence, effectively covers the entire bandwidth of ^{15}N with high fidelity. This new method will expand the application of metabolomics for analyzing amides, amines, and imines in cell extracts, especially at high and ultra-high magnetic fields.

ASSOCIATED CONTENT

Supporting Information

Supporting Figures S1-S7.

Software Availability

RF shapes and pulse sequences are available from GitHub (https://github.com/manuvsub/BB-NHSQC) and DRUM repository site at the University of Minnesota (https://hdl.handle.net/11299/166578), and via NMRFAM.

AUTHOR INFORMATION

Corresponding Author

Gianluigi Veglia — Department of Biochemistry, Molecular Biology & Biophysics, University of Minnesota, 55455 Minneapolis, Minnesota 55455, United States; orcid.org/0000-0002-2795-6964; Email: vegli001@umn.edu

Present Addresses

†If an author's address is different than the one given in the affiliation line, this information may be included here.

Author Contributions

Manu V.S.: Methodology, RF pulse generation, Original Draft. Marco Tonelli: Methodology, Data Acquisition, Data Analysis, Original Draft. Bailey Bell: Sample Preparation, Original Draft. Alok K. Sharma: Sample Preparation, Original Draft. Tim Bugni: Conceptualization, Gianluigi Veglia: Conceptualization, Funding acquisition, Data Analysis, Validation, Original Draft, Editing and reviewing final draft.

Conflict of Interest Disclosure

Gianluigi Veglia and Manu V.S. are the founders of Kantika LLC.

ACKNOWLEDGMENT

This work was supported by the U.S. National Science Foundation (CHE-2304829) and by the Office of Discovery and Translation (ODAT) at the University of Minnesota. This study made use of the National Magnetic Resonance Facility at Madison, an NIH Biomedical Technology Research Resource Center NIH R24GM141526. Helium recovery equipment, computers, and infrastructure for data archive were funded by the University of Wisconsin-Madison, NIH R24GM141526. AKS was supported in part with federal funds from the National Cancer Institute, National Institutes of Health contract 75N91019D00024. We thank the Protein Expression Laboratory (Frederick National Laboratory for Cancer Research) for their assistance in cloning, expressing and purifying of the recombinant protein.

REFERENCES

1. Emwas, A. H.; Roy, R.; McKay, R. T.; Tenori, L.; Saccenti, E.; Gowda, G. A. N.; Raftery, D.; Alahmari, F.; Jaremko, L.; Jaremko, M.; Wishart, D. S., NMR Spectroscopy for Metabolomics Research. *Metabolites* **2019,** *9* (7).
2. Letertre, M. P. M.; Giraudeau, P.; de Tullio, P., Nuclear Magnetic Resonance Spectroscopy in Clinical Metabolomics and Personalized Medicine: Current Challenges and Perspectives. *Front Mol Biosci* **2021,** *8*, 698337.
3. Morgan, K. D., The use of nitrogen-15 in microbial natural product discovery and biosynthetic characterization. *Front Microbiol* **2023,** *14*, 1174591.
4. Fei, Q.; Wang, D.; Jasbi, P.; Zhang, P.; Nagana Gowda, G. A.; Raftery, D.; Gu, H., Combining NMR and MS with Chemical Derivatization for Absolute Quantification with Reduced Matrix Effects. *Anal Chem* **2019,** *91* (6), 4055-4062.
5. Bhinderwala, F.; Lonergan, S.; Woods, J.; Zhou, C.; Fey, P. D.; Powers, R., Expanding the Coverage of the Metabolome with Nitrogen-Based NMR. *Anal Chem* **2018,** *90* (7), 4521-4528.
6. Subrahmanian, M. V.; Pavuluri, K.; Olivieri, C.; Veglia, G., High-fidelity control of spin ensemble dynamics via artificial intelligence: from quantum computing to NMR spectroscopy and imaging. *PNAS Nexus* **2022,** *1* (4), pgac133.
7. Veglia, G.; Manu, V. S., System and method for producing radiofrequency pulses in magnetic resonance using an optimal phase surface. **2022,** *PT US20200341084*.
8. Kramer, J.; Ozkaya, O.; Kummerli, R., Bacterial siderophores in community and host interactions. *Nat Rev Microbiol* **2020,** *18* (3), 152-163.
9. Smith, M.; Hernandez, J. S.; Messing, S.; Ramakrishnan, N.; Higgins, B.; Mehalko, J.; Perkins, S.; Wall, V. E.; Grose, C.; Frank, P. H.; Cregger, J.; Le, P. V.; Johnson, A.; Sherekar, M.; Pagonis, M.; Drew, M.; Hong, M.; Widmeyer, S. R. T.; Denson, J. P.; Snead, K.; Poon, I.; Waybright, T.; Champagne, A.; Esposito, D.; Jones, J.; Taylor, T.; Gillette, W., Producing recombinant proteins in Vibrio natriegens. *Microb Cell Fact* **2024,** *23* (1), 208.
10. Sharma, A. K.; Dyba, M.; Tonelli, M.; Smith, B.; Gillette, W. K.; Esposito, D.; Nissley, D. V.; McCormick, F.; Maciag, A. E., NMR (1)H, (13)C, (15)N backbone resonance assignments of the T35S and oncogenic T35S/Q61L mutants of human KRAS4b in the active, GppNHp-bound conformation. *Biomol NMR Assign* **2022,** *16* (1), 1-8.

11. Sharma, A. K.; Pei, J.; Yang, Y.; Dyba, M.; Smith, B.; Rabara, D.; Larsen, E. K.; Lightstone, F. C.; Esposito, D.; Stephen, A. G.; Wang, B.; Beltran, P. J.; Wallace, E.; Nissley, D. V.; McCormick, F.; Maciag, A. E., Revealing the mechanism of action of a first-in-class covalent inhibitor of KRASG12C (ON) and other functional properties of oncogenic KRAS by (31)P NMR. *J Biol Chem* **2024,** *300* (2), 105650.

12. Delaglio, F.; Grzesiek, S.; Vuister, G. W.; Zhu, G.; Pfeifer, J.; Bax, A., NMRPipe: a multidimensional spectral processing system based on UNIX pipes. *J Biomol NMR* **1995,** *6* (3), 277-93.

13. Kay, L. E.; Keifer, P.; Saarinen, T., Pure Absorption Gradient Enhanced Heteronuclear Single Quantum Correlation Spectroscopy with Improved Sensitivity. *J Am Chem Soc* **1992,** *114* (26), 10663-10665.

14. Palmer, A. G.; Cavanagh, J.; Wright, P. E.; Rance, M., Sensitivity improvement in proton-detected two-dimensional heteronuclear correlation NMR spectroscopy. *J Magn Reson* **1991,** *93* (1), 151-170.

15. Silver, M. S.; Joseph, R. I.; Hoult, D. I., Highly Selective Pi/2 and Pi-Pulse Generation. *Journal of Magnetic Resonance* **1984,** *59* (2), 347-351.

16. Baum, J.; Tycko, R.; Pines, A., Broadband and adiabatic inversion of a two-level system by phase-modulated pulses. *Phys Rev A Gen Phys* **1985,** *32* (6), 3435-3447.

17. Sarkar, S.; Purusottam, R. N.; Kumar, A.; Khaneja, N., Chirp pulse sequences for broadband pi rotation. *J Magn Reson* **2021,** *328*, 107002.

18. Markley, J. L.; Bruschweiler, R.; Edison, A. S.; Eghbalnia, H. R.; Powers, R.; Raftery, D.; Wishart, D. S., The future of NMR-based metabolomics. *Curr Opin Biotechnol* **2017,** *43*, 34-40.

19. Lysak, D. H.; Wolff, W. W.; Soong, R.; Bermel, W.; Kupce, E. R.; Jenne, A.; Biswas, R. G.; Lane, D.; Gasmi-Seabrook, G.; Simpson, A., Application of (15)N-Edited (1)H-(13)C Correlation NMR Spectroscopy horizontal line Toward Fragment-Based Metabolite Identification and Screening via HCN Constructs. *Anal Chem* **2023,** *95* (32), 11926-11933.

20. Manu, V. S.; Olivieri, C.; Pavuluri, K.; Veglia, G., Design and applications of water irradiation devoid RF pulses for ultra-high field biomolecular NMR spectroscopy. *Phys Chem Chem Phys* **2022,** *24* (31), 18477-18481.

21. Manu, V. S.; Olivieri, C.; Veglia, G., Water irradiation devoid pulses enhance the sensitivity of (1)H,(1)H nuclear Overhauser effects. *J Biomol NMR* **2023,** *77* (1-2), 1-14.

The data used in this paper will be available from the repository site at the University of Minnesota DRUM [https://conservancy.umn.edu/collections/6c548d8b-0f3a-4f6b-b16e-4154c88136c0] and will be accessed publicly.